Electronic Supplementary Material (ESI) for Journal of Materials Chemistry A.
This journal is © The Royal Society of Chemistry 2022

Supporting Information

Heterogeneous Ni-MOF/V_2CT_x-MXene Hierarchically-Porous Nanorods for Robust and High Energy Density Hybrid Supercapacitors

Xifeng Yang,[§,a,b] Yuhui Tian,[§,c] Shuang Li, [*,a,b] Ya-Pan Wu,[a,b] Qichun Zhang,[d] Dong-Sheng Li [*,a,b] and Shanqing Zhang [*,c]

[a] *College of Materials and Chemical Engineering, Key Laboratory of Inorganic Nonmetallic Crystalline and Energy Conversion Materials, China Three Gorges University, Yichang 443002, P. R. China*

[b] *Hubei Three Gorges Laboratory, Yichang, Hubei 443007, P. R. China*

[c] *Centre for Catalysis and Clean Energy, School of Environment and Science, Gold Coast Campus, Griffith University, Gold Coast, Queensland 4222, Australia.*

[d] *Department of Materials Science and Engineering, City University of Hong Kong, Kowloon, Hong Kong SAR, China.*

[§] *Xifeng Yang and Yuhui Tian contributed equally to this work.*

E-mail: lishmail@126.com; lidongsheng1@126.com; s.zhang@griffith.edu.au

Material characterization

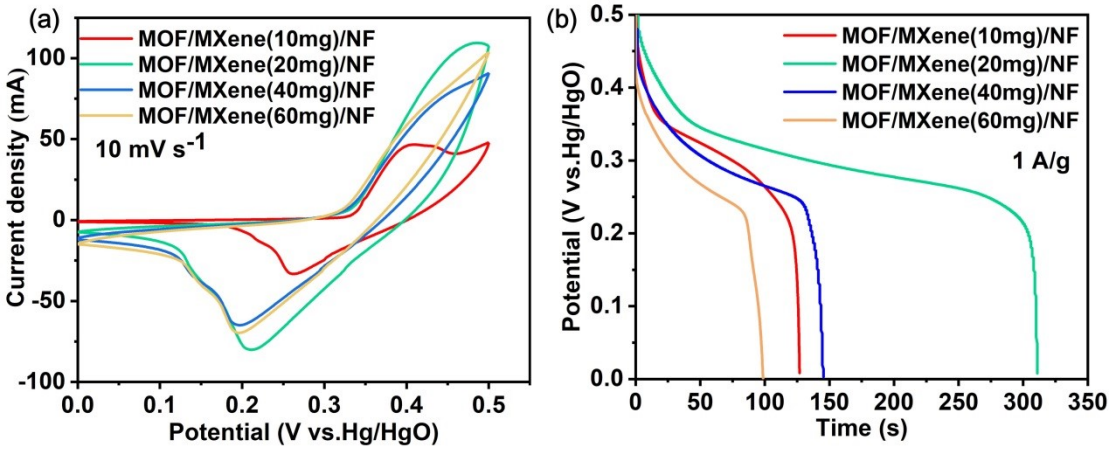

Fig. S1 (a) CV and (b) GCD curves of MOF/MXene/NF composites with different MXene loading amount. By comparison, the performance-optimal MOF/MXene/NF composite with 20 mg MXene loading amount was chose as precursor for the followed annealing treatment.

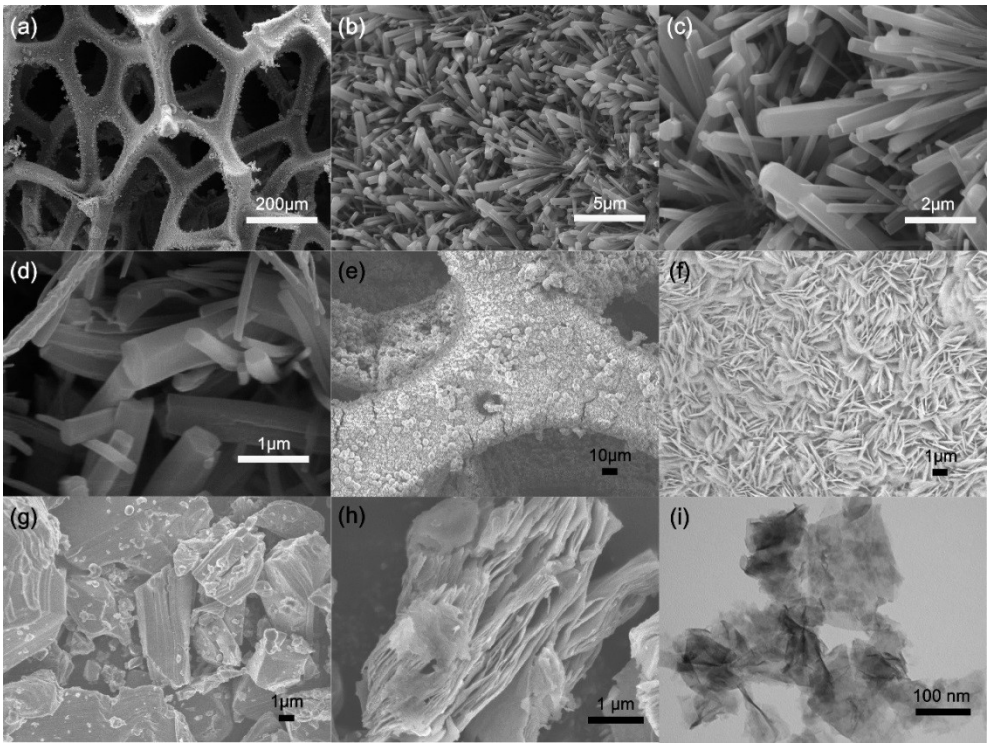

Fig. S2 (a-d) SEM images at different magnification rates of the MOF/MXene/NF. (e) Low and (f) high magnification SEM images of Ni-BDC/NF. (g) SEM images of the pristine V_2AlC. (h) Layered V_2CT_x. (i) TEM image of the as-exfoliated V_2CT_x nanosheets.

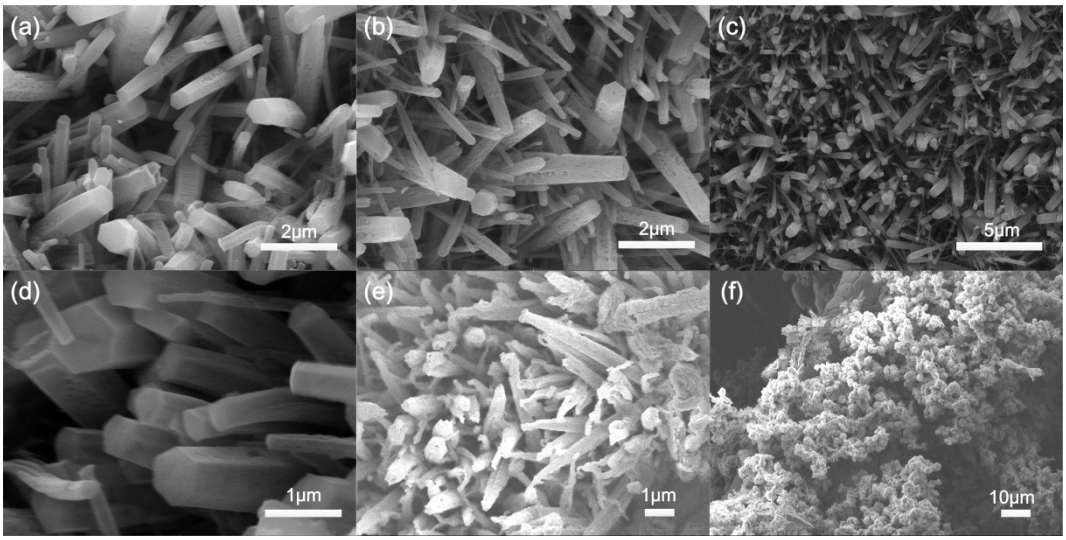

Fig. S3 (a) SEM images of the MOF/MXene/NF-150. (b) SEM of the Ni-MOF/NF-200. (c) Low and (d) high magnification SEM images of MOF/MXene/NF-300. (e) The SEM image of the MOF/MXene/NF-350. (f) The SEM image of the MOF/MXene/NF-380.

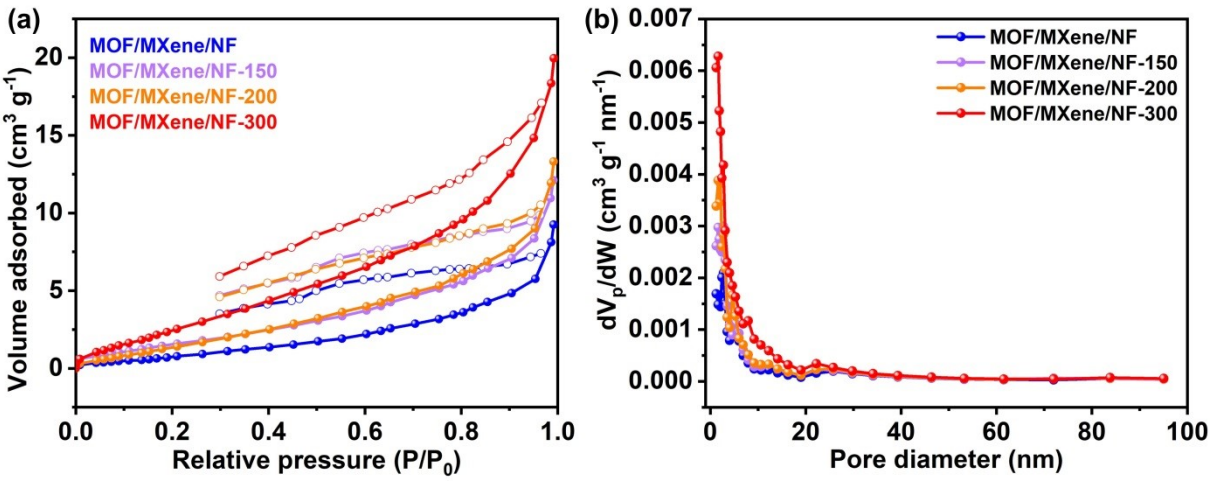

Fig. S4 (a) N_2 adsorption-desorption isotherm and (b) pore-size distribution curve of the four samples.

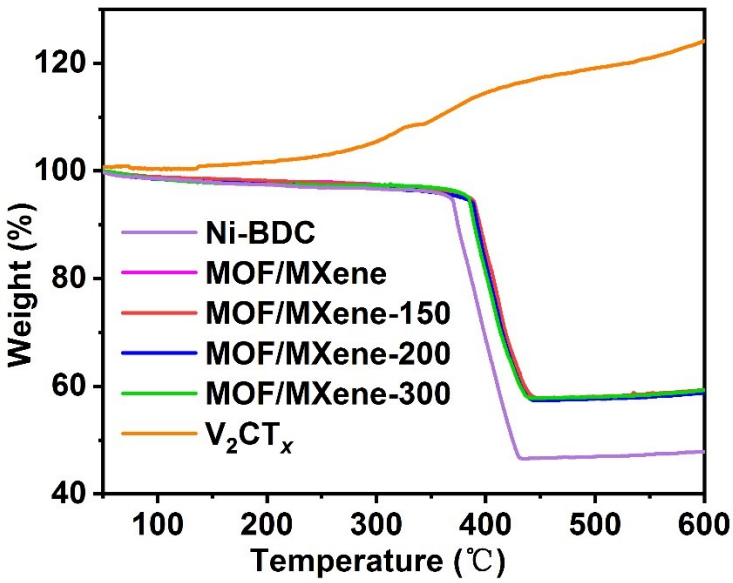

Fig. S5 TG curves of the powdered samples.

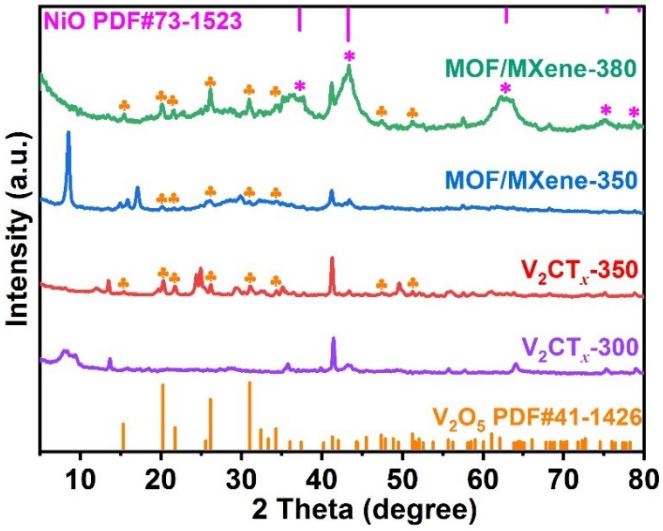

Fig. S6 XRD patterns of the powdered V_2CT_x-300, V_2CT_x-350, MOF/MXene-350 and MOF/MXene-380. It can be seen that the structure of V_2CT_x is still kept at 300 ℃ and the structure of MOF is maintained below 350 ℃.

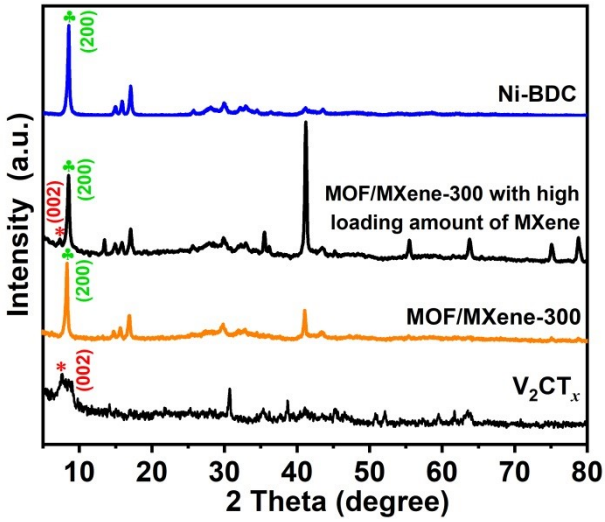

Fig. S7 The XRD patterns of the collected MOF/MXene-300 powders. Although no obvious diffraction peaks for V_2CT_x are observed in target composite (MOF/MXene-300) due to the low loading amount, the characteristic (002) peak at 7.4° of V_2CT_x and (200) peak at 8.9 of Ni-BDC can be clearly seen in the XRD pattern of MOF/MXene-300 with high loading amount of MXene, directly confirming the co-existence of MXene and MOF in the composite.

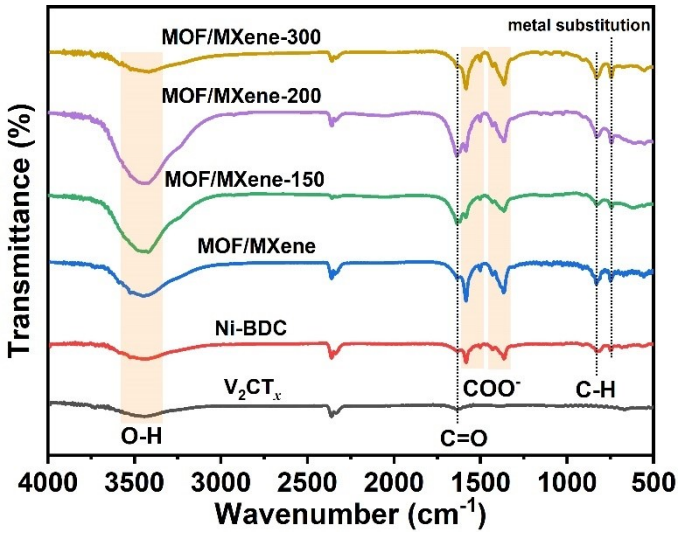

Fig. S8 FT-IR spectra of the collected powder samples. These FTIR spectra show a broad peak between 3200–3600 cm^{-1}, which can be assigned to the stretching vibration of O–H. The characteristic vibration at 1630 cm^{-1} corresponding to the C=O for V_2CT_x and Ni-BDC. Furthermore, there are some sharp peaks in the regions of 1490–1600 cm^{-1} and 1350–1450 cm^{-1}, which belong to the asymmetric and symmetric stretching vibrations of the carboxyl group, respectively. In addition, the IR band at 830 cm^{-1} is the characteristic aromatic CH stretching vibration. The IR band located at 744 cm^{-1} can be indexed to the metal substitution on benzene groups. Based on the above analysis, the absorption bands of MOF/MXene are almost identical to those of Ni-BDC and V_2CT_x in the IR spectrum, which proves that MOF/MXene is successfully formed.

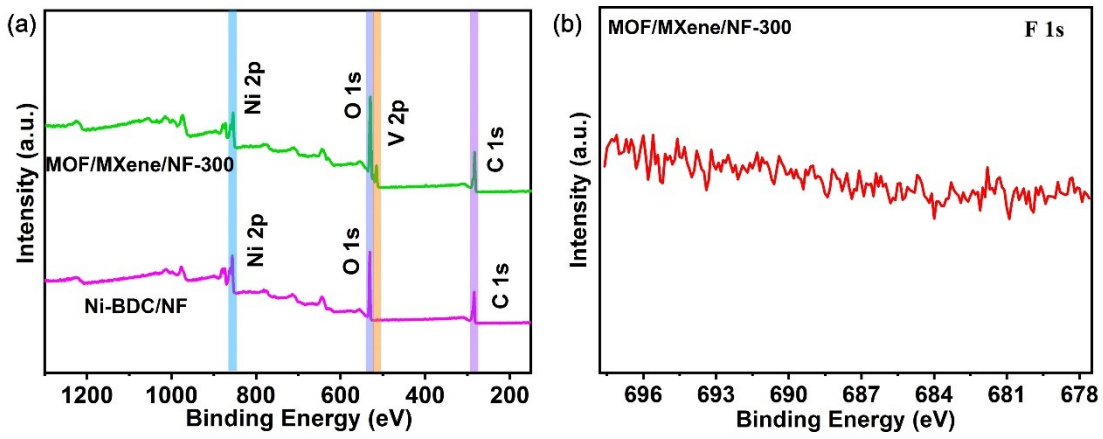

Fig. S9 (a) XPS survey spectra of the Ni-BDC/NF and MOF/MXene/NF-300. (b) F 1s spectra of the MOF/MXene/NF-300.

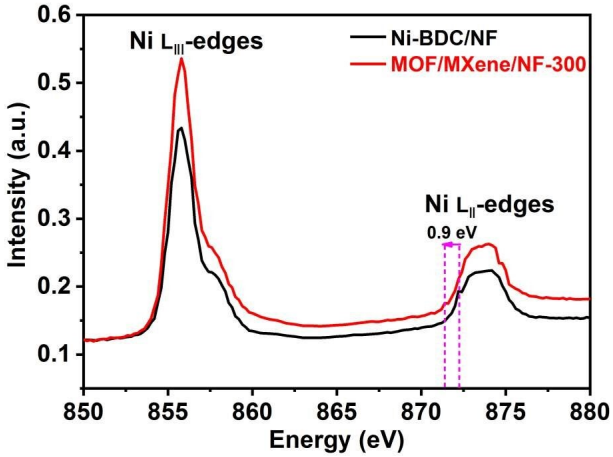

Fig. S10 Ni L-edge XANES spectra of the samples.

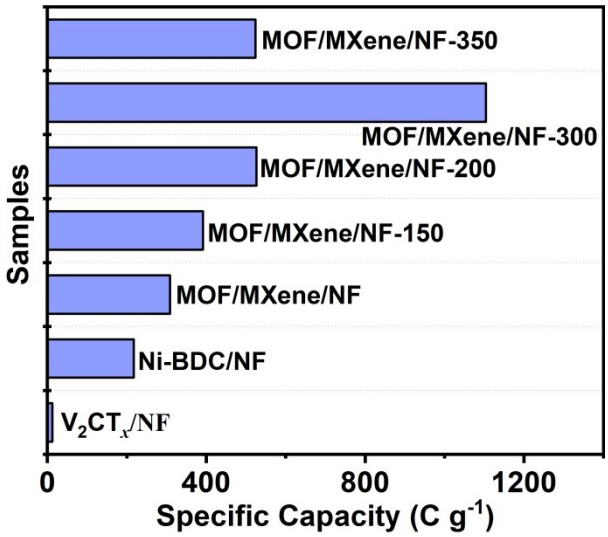

Fig. S11 Specific capacity comparison of the samples at 1 A g^{-1}.

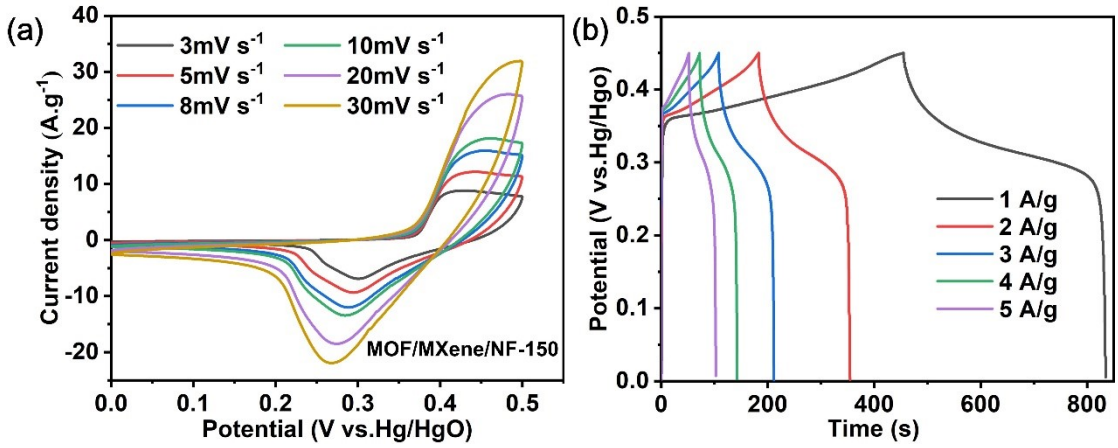

Fig. S12 (a) CV curves of MOF/MXene/NF-150 at different scan rates. (b) GCD curves of MOF/MXene/NF-150 at different current densities.

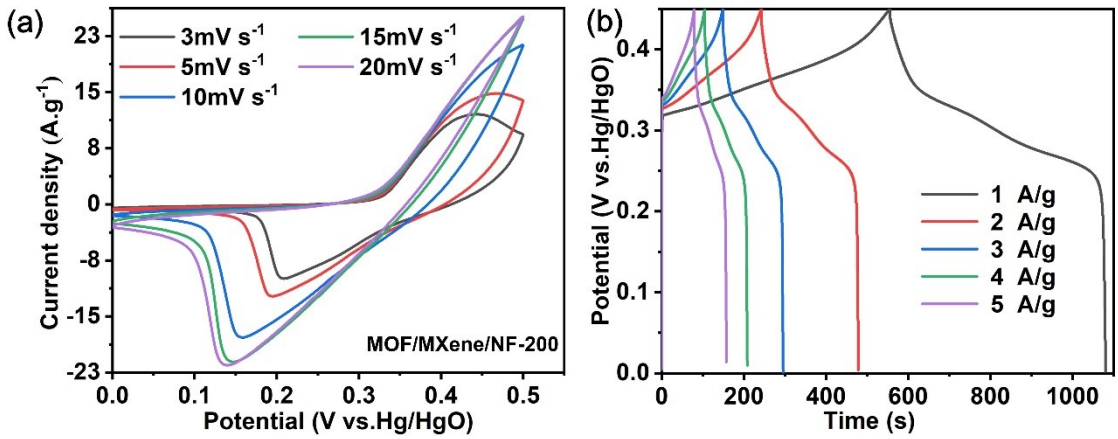

Fig. S13 (a) CV curves of MOF/MXene/NF-200 at different scan rates. (b) GCD curves of MOF/MXene/NF-200 at different current densities.

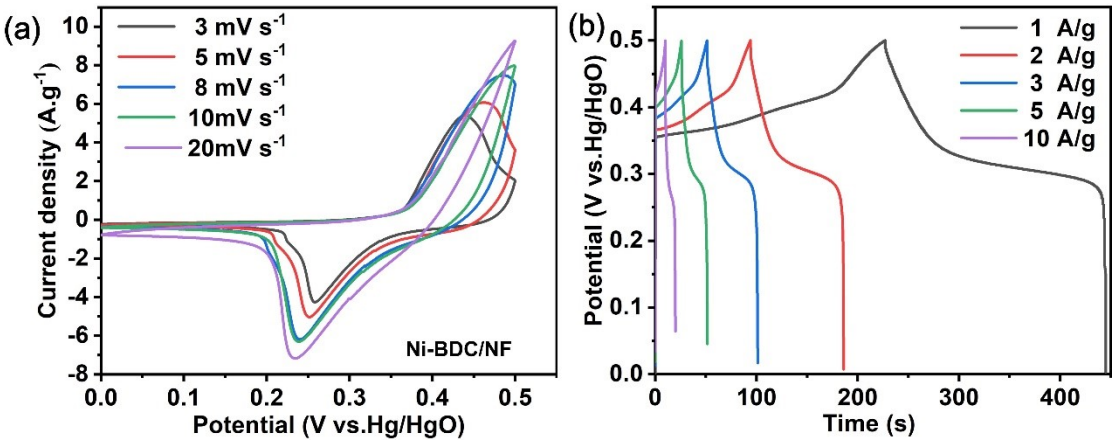

Fig. S14 (a) CV curves of Ni-BDC/NF at different scan rates. (b) GCD curves of Ni-BDC/NF at different current densities.

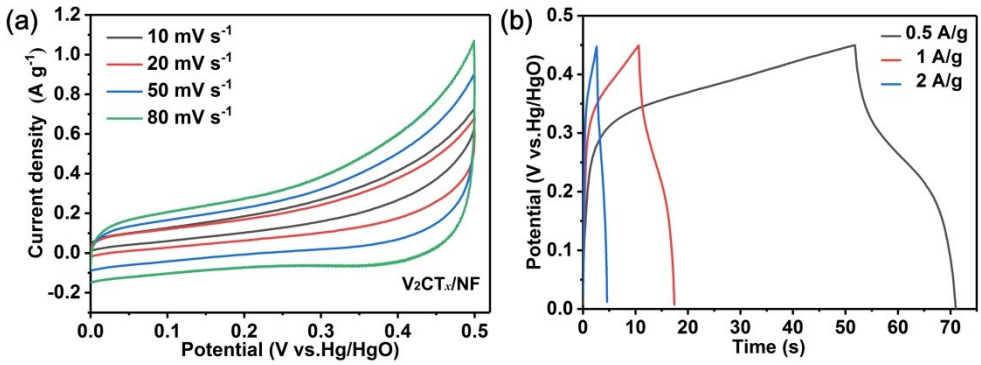

Fig. S15 (a) CV curves of V_2CT_x/NF at different scan rates. (b) GCD curves of V_2CT_x at different current densities.

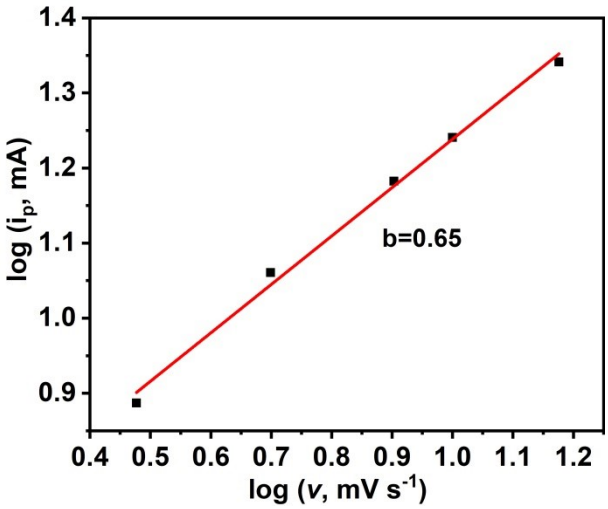

Fig. S16 The cathodic peaks current density as a function of square root of scan rate for the CoTC-300.

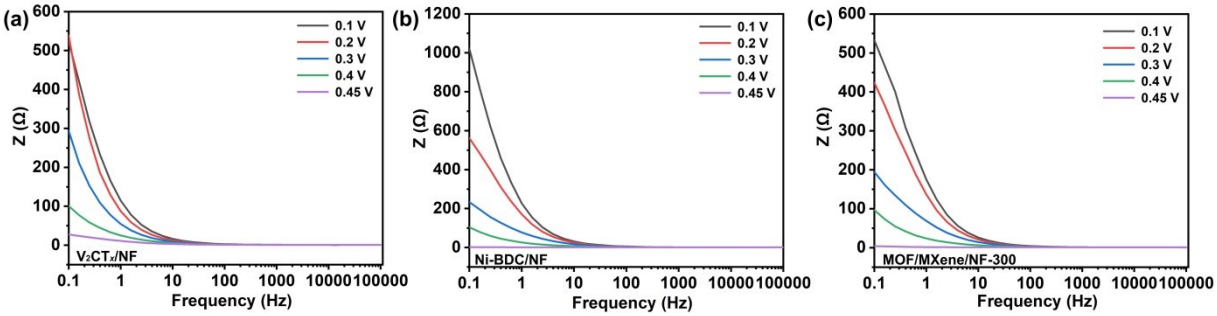

Fig. S17 The Bode phase angle plot of the (a) V_2CT_x/NF (b) Ni-BDC/NF and (c) MOF/MXene/NF-300 electrodes as a function of applied frequency.

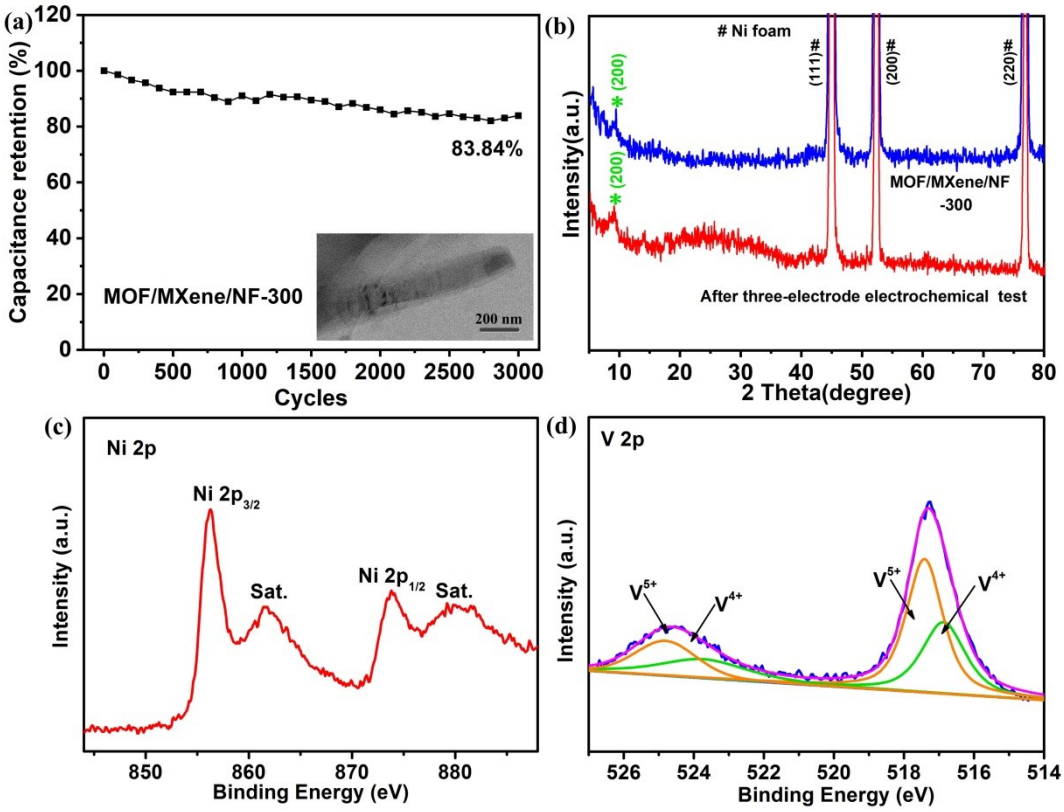

Fig. S18 (a) The cyclic stability of the three-electrode test for MOF/MXene/NF-300. The inset in (a) is the TEM image, (b) XRD pattern, (c) Ni 2p XPS and (d) V 2p XPS of MOF/MXene/NF-300 after cycling stability test.

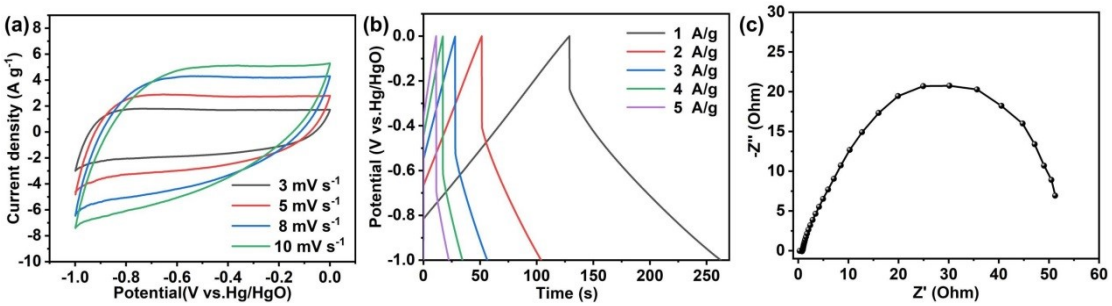

Fig. S 19 (a) The CV curves and (b) GCD curves and (c) EIS of the activated carbon/NF.

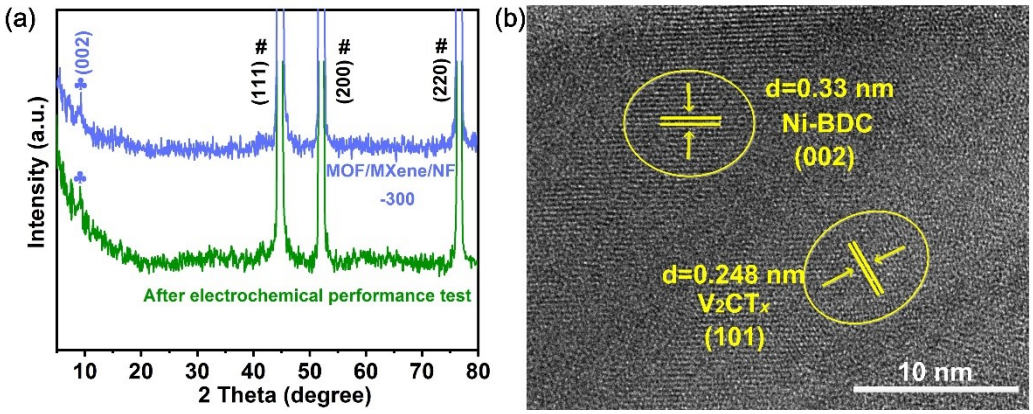

Fig. S20 Characterizations of the MOF/MXene/NF-300 after electrochemical performance test: (a) XRD. (b) HRTEM.

Table S1. Comparison of the relevant electrochemical parameters and performances of the optimal electrode and the other similar materials.

Electrode materials	Electrolyte	Current collector	Potential window /V	Capacitance/F g^{-1}	Capacity/C g^{-1}	Stability in % Retention (number of cycles)	Highest Energy Density /Wh kg^{-1}	Highest Power Density /W kg^{-1}	Cathode Materials to assemble device	Ref.
MOF/MXene /NF-300	1 M KOH	nickel foam	1.5	2453	1103.9	118.1% (15 000)	46.3	746.8	AC	this work
Ni-MOF	6 M KOH	nickel foam		1148	459.2	90% (2000)				1
NiCo-MOF	2 M KOH	nickel foam	1.5	1202.1	601.05	76.7% (5000)	49.4	562.5	AC	2
Ni/Co-MOF	1 M LiOH	glassy carbon		530.4	265.2	99.75% (2000)				3
T-Nb_2O_5	1 M $LiClO_4$	copper foil		169.23	330					4
Ni–S/d-Ti_3C_2	6 M KOH	carbon cloth	1.9	1680.8	840.4	71.4% (10 000)	20	500	d-Ti_3C_2	5
Ti_3C_2/CuS	1 M KOH	nickel foam	1.5	282.5	169.5	82.4% (5000)	15.4	750.2	Ti_3C_2 MXene	6
MXene-$NiCo_2S_4$@NF	3 M KOH	nickel foam	1.6	1193.38	596.69	80.4% (3000)	27.24	0.48 k	AC	7
$NiCo_2S_4$/MXene	3 M KOH	nickel foam	1.7	2056	1028	94.27% (5000)	68.7	850	AC	8
Co-MOF@Ni	1 M KOH	nickel foam		2872.5	1149	92.1% (3000)				9
NiCoAl-LDH/$V_4C_3T_x$	1 M KOH	nickel foam	1.6	1045	627	98% (10 000)	71.7	20 000	AC	10
200-$Ti_3C_2T_x$	1 M H_2SO_4	MXene films	0.7	429	300.3	89% (5000)	29.2	390	200-$Ti_3C_2T_x$	11
d-Ti_3C_2/NF	6 M KOH	nickel foam	1.3	654	327	80.6% (5000)	18.1	397.8	bulk Ti_3C_2	12
NiCo-MOF/$Ti_3C_2T_x$	2 M KOH	nickel foam	1.5	815.2	366.84	82.3% (10 000)	39.5	562.5	AC	13
$Ti_3C_2T_x$/CNTs	3 M H_2SO_4	film	1	375	300	95.9% (10 000)	9.2	96.1	$Ti_3C_2T_x$/ CNTs	14
N, O co-doped C@Ti_3C_2	6 M KOH	nickel foam	1.2	250.6	200.48	94% (5000)	10.8	600	N, O co-doped C@Ti_3C_2	15

Table S2 The diffusion coefficient values of all the electrodes in KOH electrolyte

	V_2CT_x/NF	Ni-BDC/NF	MOF/MXene/NF	MOF/MXene/NF-150	MOF/MXene/NF-200	MOF/MXene/NF-300	MOF/MXene/NF-350
Diffusion coefficient D, (cm^2 s^{-1})	2.84473E-14	8.41208E-15	1.05211E-14	1.58042E-14	1.62229E-14	1.76897E-14	1.36537E-13

References

1 X. Xiong, L. Zhou, W. Cao, J. Liang, Y. Wang, S. Hu, F. Yu and B. Li, *CrystEngComm*, 2017, **19**, 7177-7184.

2 Y. Wang, Y. Liu, H. Wang, W. Liu, Y. Li, J. Zhang, H. Hou and J. Yang, *ACS Appl. Energy Mater.*, 2019, **2**, 2063-2071.

3 H. Xia, J. Zhang, Z. Yang, S. Guo, S. Guo and Q. Xu, *Nano-Micro Lett.*, 2017, **9**, 43.

4 C. Zhang, M. Beidaghi, M. Naguib, M. R. Lukatskaya, M.-Q. Zhao, B. Dyatkin, K. M. Cook, S. J. Kim, B. Eng, X. Xiao, D. Long, W. Qiao, B. Dunn and Y. Gogotsi, *Chem. Mater.*, 2016, **28**, 3937-3943.

5 Y. Luo, C. Yang, Y. Tian, Y. Tang, X. Yin and W. Que, *J. Power Sources*, 2020, **450**, 227694.

6 Z. Pan, F. Cao, X. Hu and X. Ji, *J. Mater. Chem. A.*, 2019, **7**, 8984-8992.

7 H. Li, X. Chen, E. Zalnezhad, K. N. Hui, K. S. Hui and M. J. Ko, *J. Ind. Eng. Chem.*, 2020, **82**, 309-316.

8 J. Fu, L. Li, J. M. Yun, D. Lee, B. K. Ryu and K. H. Kim, *Chem. Eng. J.*, 2019, **375**, 121939.

9 R. Ramachandran, K. Rajavel, W. Xuan D. Lin and F. Wang, *Ceram. Int.*, 2018, **44**, 14425-14431.

10 X. Wang, H. Li, H. Li, S. Lin, J. Bai, J. Dai, C. Liang, X. Zhu, Y. Sun and S. Dou, *J. Mater. Chem. A.*, 2019, **7**, 2291-2300.

11 Z. Zhang, Z. Yao, X. Zhang and Z. Jiang, *Electrochim. Acta*, 2020, **359**, 136960.

12 J. Guo, Y. Zhao, A. liu and T. Ma, *Electrochim. Acta*, 2019, **305**, 164-174.

13 Y. Wang, Y. Liu, C. Wang, H. Liu, J. Zhang, J. Lin, J. Fan, T. Ding, J. E. Ryu and Z. Guo, *Eng. Sci.*, 2020, **9**, 50-59.

14 P. Zhang, Q. Zhu, R. A. Soomro, S. He, N. Sun, N. Qiao and B. Xu, *Adv. Funct. Mater.*, 2020, **30**, 2000922.

15 Z. Pan and X. Ji, *J. Power Sources*, 2019, **439**, 227068.